Near surface magnetic domain observation with ultra-high resolution

Zhenghua. Li[1], Xiang Li[2], Dongping Liu[1*], H. Saito[3] and S. Ishio[4]

Author affiliations: [1]Liaoning Key Lab of Optoelectronic Films & Materials, School of Physics and Materials Engineering, Dalian Nationalities University, Dalian, 116600, China; [2]School of Materials Science and Engineering, University of Shanghai for Science and Technology, Shanghai, 200093, China; [3]Research Center for Engineering Science, Graduate School of Engineering & Resource Science, Akita University, Gakuen Machi 1-1, Tegata, Akita, 010-8502, Japan; [4]Venture Business Laboratory, Akita University, Gakuen Machi 1-1, Tegata, Akita, 010-8502, Japan

Corresponding person: Dongping Liu (phone: +86-411-87508902, fax: +86-411-87508902, email: dongping.liu@dlnu.edu.cn)

SECTION 1： The details of the MFM tip and ferrite core

In NF-MFM, the soft $Ni_{90}Fe_{10}$ MFM tip was prepared by a radio-frequency (RF) magnetron sputtering system. A commercial Si tip (Made in SII Nanotechnology, spring constant is 20 N/m) was used as a base tip. The NiFe film was deposited on the Si tip at room temperature using a hybrid target consisting of Fe chips placed on Ni disc. The base pressure of this system was lower than 3×10^{-7} Torr, and the Ar gas pressure was 3.75 mTorr during the film deposition. The sputtering power and time were held at 200 W and 60 seconds, respectively. After the magnetic material deposition, the NiFe-coated tip was annealed at 400 °C for 1 h in the ultra-high vacuum chamber to improve the soft magnetic properties.

Figure S1 shows the geometry and dimensions of the ferrite core. The materials of the ferrite core are Fe_2O_3 (50%), NiO (24%) and ZnO (26 %). The initial permeability (μ_i), maximum flux density (B_m), remanence (B_r) and coercivity (H_c) of the ferrite core are 750, 350 mT, 100 mT, 25 A/m, respectively.

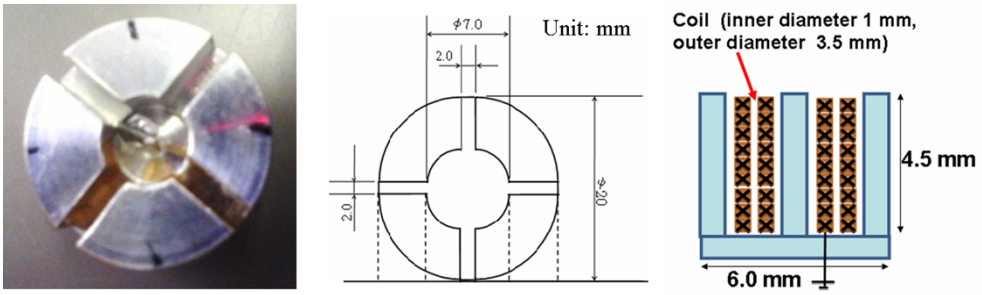

Figure S1 The geometry and dimensions of the ferrite core.

SECTION 2： The quantification of static magnetic field from the recording bits

One way to understand the magnetic field characteristic is to compare the measured MFM images with the simulated ones. Here, we demonstrate a deconvolution technique to quantify the magnetic fields from recording bits.

The measured MFM signal is considered as the convolution of the magnetized surface and the tip's sensitivity field, and this can be mathematically represented as follows

$$\varphi(x,y,z_0) = \iint_{x',y'} G_\rho(x-x',y-y',z_0)\rho(x',y')dx'dy' \qquad \text{(S1)}$$

where $\varphi(x,y,z_0)$ is the force gradients, and $G_\rho(x-x',y-y',z_0)$ the MFM tip Green's function.

Taking the Fourier transform of both sides of equation (S1), the following expression for the magnetic pole density distribution can be derived,

$$\rho(x,y) = F^{-1}\left\{\frac{\varphi(k_x,k_y)}{G_\rho(k_x,k_y)}\right\} = \rho_{\max}\cdot\rho_i(x,y) \qquad \text{(S2)}$$

where k_x , k_y are the components of the wave vector in Fourier space, $\rho_{\max}$ the maximum magnetic charge density, and ρ_i the normalized magnetic charge in the *i*th cuboid mesh. The value of $\rho_{\max}$ is determined by $M_n \Big/ \left[\frac{1}{N_{grids}}\sum_i \rho_i\right]$, where N_{grids} is the number of grids or meshes, and M_n the perpendicular magnetization calibrated by a vibrating-sample magnetometer.

By using the ‘‘magnetic dipole approximation’’ and assuming that the measurement is done with the constant tip–sample space, the three-dimensional

Green's function of for a point magnetic dipole tip with respect to a point magnetic charge can be obtained in the frequency domain [35,40],

$$G_\rho(k_x,k_y,z) = -\frac{m_x}{2\mu_0} ik_x \sqrt{k_x^2+k_y^2}\, e^{-\sqrt{k_x^2+k_y^2}z} - \frac{m_y}{2\mu_0} ik_y \sqrt{k_x^2+k_y^2}\, e^{-\sqrt{k_x^2+k_y^2}z} + \frac{m_z}{2\mu_0}(k_x^2+k_y^2) e^{-\sqrt{k_x^2+k_y^2}z} \quad \text{(S3)}$$

The two-dimensional Fast Fourier Transforms (FFTs) are used to implement this algorithm numerically. The raw image is transformed into Fourier space, then multiplied by a window function before performing the deconvolution procedure. This function is unity at the middle of the image and drops off as a Gaussian towards the image edges.

Figure S2 (a) shows the quantified perpendicular and in-plane magnetic field components near the sample surface (based on the experimental result of Figure 4 (a) in main text). The magnetic field is obtained by $\vec{H}(\vec{r}) = \sum_{i=1}^{n} \frac{\rho_{\max}}{4\pi\mu_0} \frac{\rho_i(\vec{r}')(\vec{r}-\vec{r}')}{|\vec{r}-\vec{r}'|^3}$. The color in Figure S2 (a) shows the magnitude and direction of perpendicular component (z component, H_z) of magnetic field, while the vectors represent the direction and value of in-plane components of surface magnetic field (the value varies between 0 to 90 Oe). It is noted that there is a big difference between the quantified perpendicular field (H_z) and the measured one in Figure 4 (a) in main text showing sharp edges. The big difference can be well characterized as the perpendicular magnetic field (H_z) compared with its field gradients, where the measured MFM signals are considered to

be proportional to the field gradients ($\frac{\partial^2 H_z}{\partial z^2}$). Figure S2 (b) shows the simulated MFM image based on the quantified results of Figure S2 (a). By working out the second order derivative $\frac{\partial^2 H_z}{\partial z^2}$ above a head surface, the calculated MFM image agrees well with the measured MFM image (Figure 4(a) in main text).

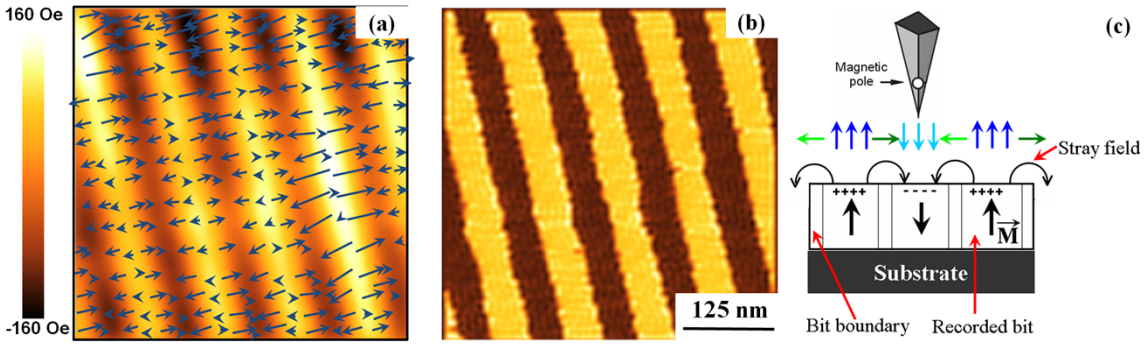

Figure S2 (a) The quantified perpendicular and in-plane magnetic field components near sample surface, (b) the calculated magnetic field gradient map, (c) the schematic drawing of magnetic field near the surface of the recording medium.

SECTION 3： The imaging of the irregular structure by NF-MFM

We have imaged the irregular structure ($La_{0.7}Sr_{0.3}MnO_3$ granular film) by near field magnetic force microscopy (NF-MFM), as shown in Figure S3. The experiment was conducted at a lift height of -20 nm. The driven frequency and intensity of the ferrite core are 30 Hz and 150 Oe, respectively. The sample is a polycrystalline $La_{0.7}Sr_{0.3}MnO_3$ granular film with a nonmagnetic grain boundary phase. The sample was magnetized in the horizontal direction with an in-plane magnetic field of 800 Oe. Figure S3 (a) shows a topographic image of the polycrystalline $La_{0.7}Sr_{0.3}MnO_3$ film

with a granular structure. The magnetic grains, clusters, and the nonmagnetic grain boundary phase can be clearly observed. Figure S3 (b) shows the perpendicular component of static magnetic field gradients at sample surface, the areas at nonmagnetic grain boundaries show the neighboring bright-dark contrast. Figure S3 (c) shows the in-plane component of static magnetic field gradients, only bright contrast appears at the grain boundaries. In the case of the $La_{0.7}Sr_{0.3}MnO_3$ film in the magnetized state, the maximum and minimum intensities of perpendicular field gradients are obtained at the edges of neighboring magnetic grains (see dark blue and light blue arrows in Figure S3 (d), relating to the bright-dark contrast in Figure S3 (b)). However, the maximum intensities of longitudinal field gradients are captured at the grain boundaries (see green arrow in Figure S3 (d), corresponding to the bright contrast in Figure S3 (c)). Therefore, based on the NF-MFM, the 3D magnetic field gradients in the irregular structure can be characterized.

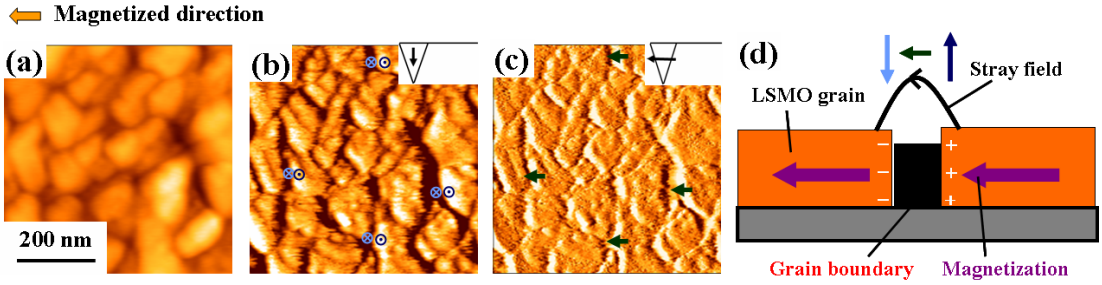

Figure S3 (a) The topographic image, (b) the NF-MFM perpendicular magnetic field gradients, (c) the NF-MFM in-plane magnetic field gradients and (d) schematic image of the $La_{0.7}Sr_{0.3}MnO_3$ film.

SECTION 4: The quantification of actual tip-sample distance

In NF-MFM measurement, two scans are taken, where one is in tapping mode (to

get the topographic contrast, the actual tip-sample distance is d_0), and the other is in lift mode (the MFM tip lift a constant distance with respect to the first scan, and the actual tip-sample distance is d) to get the magnetic contrast only. The lift height is defined as the distance between the first and second scans (lift height $D=d-d_0$). In tapping mode, only the AFM scans are carried out, and the lift height is zero. In lift mode, the MFM scans are taken by keeping a constant tip-to-sample distance. The positive value of a lift height means the MFM tip lifts further from a sample surface ($d > d_0$), while the negative value of a lift height indicates that the MFM tip gets closer to the surface of sample ($d < d_0$). In the main text, when D=-69 nm, the MFM tip just contacts the sample surface (Figure 5 (c) in main text), therefore, the actual tip-sample distance can be quantified by the lift height D (e.g. when D=-68 nm, the actual tip-sample distance is 1 nm).

SECTION 5： The determination of spatial resolution

In NF-MFM, the best resolution can be obtained when the MFM tip gets closest to the surface of sample, without contacting the surface. In NF-MFM, when the lift height D=-68 nm, the actual tip-sample distance is only 1 nm, in this case, the MFM tip gets closest to the sample surface. The best resolution of 5 nm is obtained by a Fourier-based analysis of the MFM image at the lift height D=-68 nm [37], as shown in Figure S4. The figure gives the response of the MFM signal intensity as a function of spatial frequency (k_x). In the Fourier spectrum, the maximum detectable spatial frequency introduced in Reference [36] is used to evaluate the spatial resolution.

Therefore, the MFM resolution is determined by the maximum detectable frequency (k_c), where the intensity of MFM signal spectrum reduces to the white background level (thermodynamic noise of cantilever) [37]-[39]. The MFM resolution is estimated as half of the critical wavelength $\lambda_c = \frac{1}{2k_c}$. In Figure S4, the critical frequency $k_c \approx 100$ （1/μm）, therefore, the estimated resolution is 5 nm.

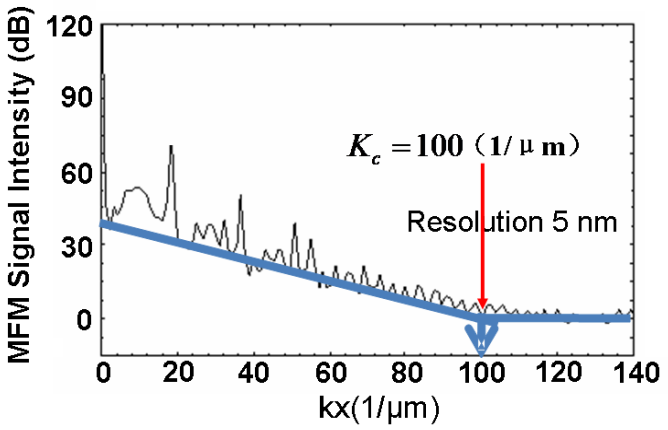

Figure S4 Fourier spectrum of the MFM signal

SECTION 6: The comparison between conventional MFM and NF-MFM images

Figure S5 shows the topographic image (a), and conventional MFM phase image (b) of the perpendicular magnetic anisotropy (PMA) material. The experiment was conducted at a lift height of -20 nm in air atmosphere. The oscillation frequency (f_c) of the piezoelectric element is near the resonant frequency (f_0) of the tip. The f_c and Q values are approximately 300 kHz and 600, respectively. Tapping and lift mode AFM/MFM scans are carried out using a high-coercivity FePt tip. In the MFM phase image of Figure S5 (b), the recorded bits can be clearly observed. Figure S5 (c) shows

the NF-MFM image taken with the same lift height, and it is seen that the signal-to-noise (S/N) ratio enhances in NF-MFM image.

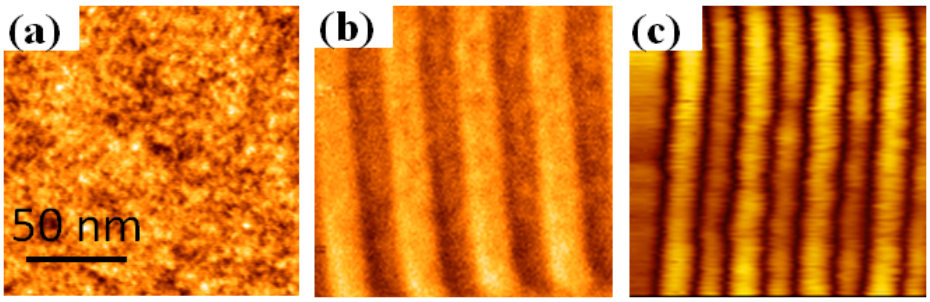

Figure S5 (a) Topographic image, (b) conventional MFM phase image, and (c) NF-MFM image of the PMA material.

SECTION 7： The imaging of the time-variable AC magnetic field from a single-pole-type (SPT) head by frequency modulated magnetic force microscopy (FM-MFM)

Figure S6 shows the schematic diagram of the FM-MFM system for imaging the AC magnetic field from SPT head. The system is based on a conventional JSPM-5400 (JEOL Ltd.) scanning probe microscope. In FM-MFM, the cantilever is oscillated by a piezoelectric element, and the AC magnetic field from the writing head causes the FM of the cantilever oscillation. The FM-MFM signal of the cantilever oscillation is sensed by a photo detector with a laser beam deflection technique and is demodulated using a phase locked loop (PLL) circuit (easyPLL, Nanosurf®). The signals out of PLL are fed into a lock-in amplifier. Here, the reference signal of the lock-in amplifier is the AC voltage used to drive the SPT head. The experiment was conducted in an air atmosphere. The oscillation frequency of the piezoelectric element was near the

resonant frequency of the MFM tip. Tapping and lift mode AFM/MFM scans were conducted using a high-coercivity MFM FePt tip (SI-MF40-Hc, Nitto Optical Co., Ltd) with the coercivity of more than 10 kOe.

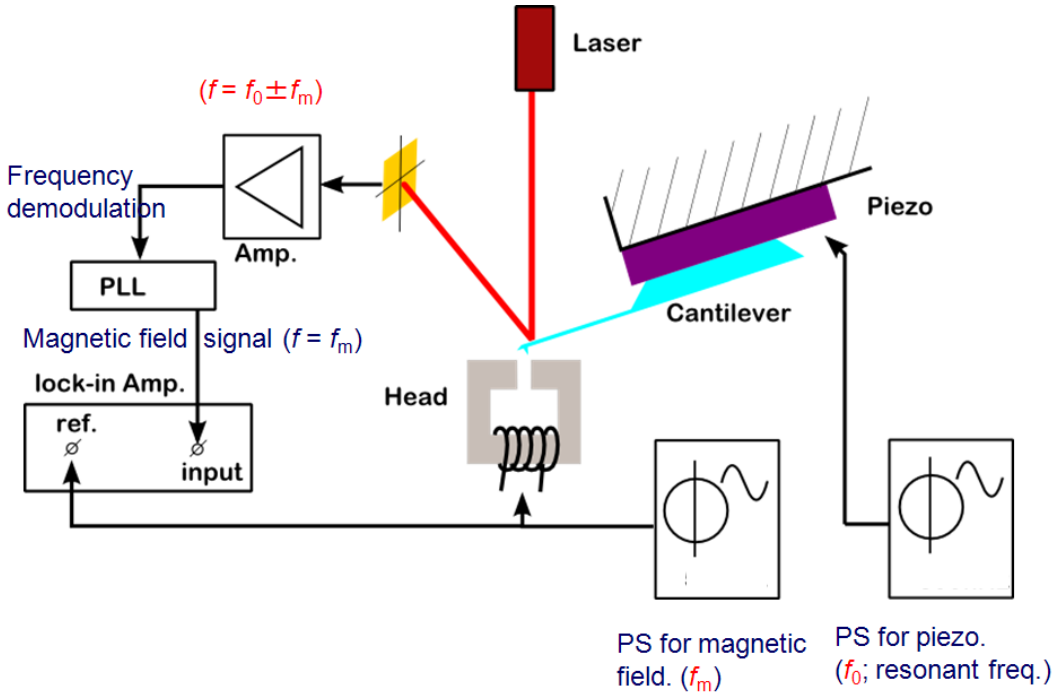

Figure S6 Schematic diagram of the FM-MFM system

The sample is a shielded single-pole-type head (SPT head). Figure S7 (a) shows the 3-Dimensional schematic structure of the SPT head. The main pole, the gap between main pole and shield, and the Air Bearing Surface (ABS, in X-Y plane, the AFM scanning plane) can be clearly seen. Figure S7 (b) shows the schematic figure of ABS plane relating to Figure S7 (a). The main pole can be easily identified. In the FM-MFM, we can detect the signal information from the ABS surface. When we capture the main pole area, we can get strong MFM contrast near the pole position.

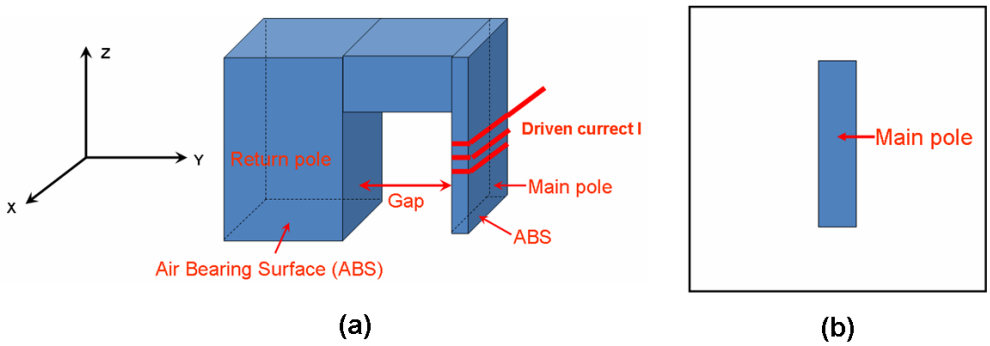

Figure S7 (a) The 3-Dimensional schematic structure of a single-pole-type (SPT) head, (b) the schematic figure of the Air Bearing Surface (ABS) relating to (a)

In the FM-MFM system, the alternating magnetic field from a recording head has a phase delay with respect to the driving head voltage due to the phase shift arising from electronics (including the RL circuit) and magnetics. By using the modulation lock-in technique, we considered the total phase shift of alternating magnetic field with respect to the head voltage and changed the phase delay by adding an extra phase (or time evolution operator $e^{i\,\omega_m \Delta t}$) to the original phase image using a lock-in amplifier [32]. Figure S8 shows the stroboscopic analysis of AC magnetic field for the SPT head. The head was driven by a sinusoidal AC current with a zero-to-peak amplitude of 20 mA and a frequency of 100 Hz. From the figure, we can observe that the MFM contrast varies periodically at the pole area (the MFM contrast changes from bright to dark, and then bright). The estimated magnetization at the main pole region is thought to rotate periodically with the modulation frequency.

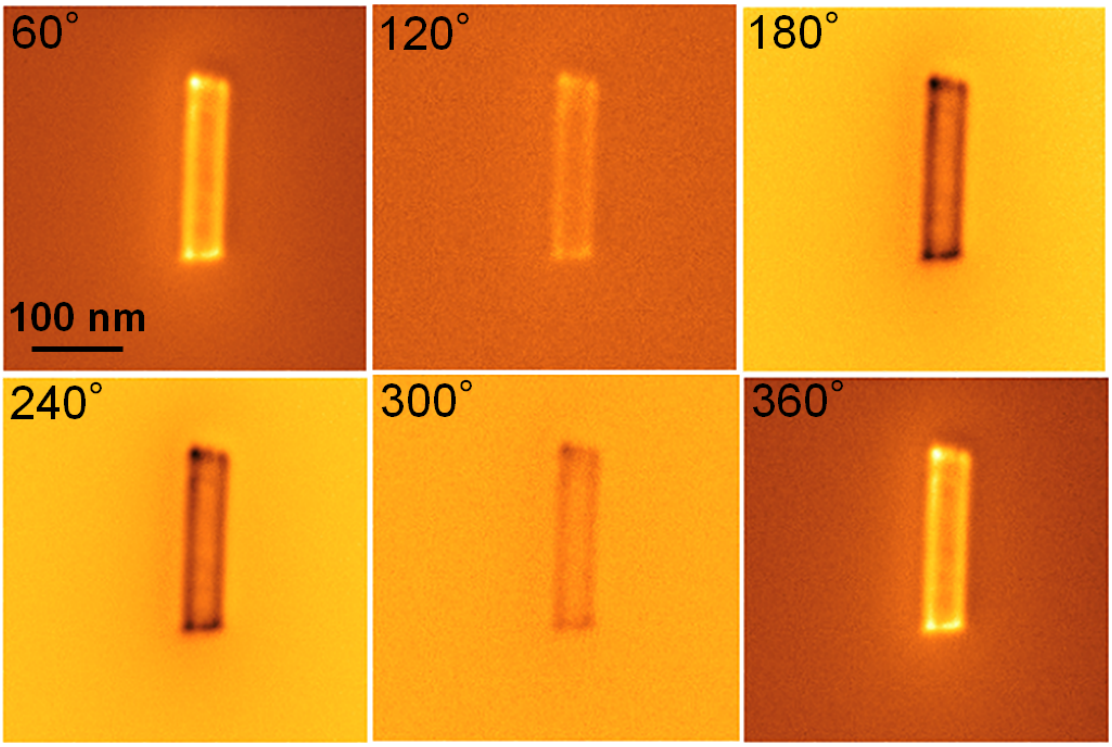

Figure S8 The stroboscopic imaging of the time-variable AC magnetic domains for the SPT head.